Nuclear Instruments and Methods in Physics Research A 353 (1994) 328–333

ELSEVIER

NUCLEAR INSTRUMENTS & METHODS IN PHYSICS RESEARCH Section A

# A high energy gamma camera using a multiple hole collimator and PSPMT ☆

S.V. Guru *, Z. He, J.C. Ferreria, D.K. Wehe, G.F. Knoll

*Department of Nuclear Engineering, The University of Michigan, Ann Arbor, MI 48109-2104, USA*

**Abstract**

A high energy gamma camera using a parallel hole tungsten collimator and a 7.62 cm square Position Sensitive Photomultiplier Tube (PSPMT) has been assembled and tested. The measured energy resolution is 12–20% FWHM for $^{137}$Cs (662 keV) gamma rays, and 17–23% FWHM for $^{57}$Co (122 keV). The measured spatial resolution measured is 2.8–3.2 mm for 122 keV and 3.4–5.3 mm for 662 keV. The variation in the energy and spatial resolution is due to the continuously varying gain across the PSPMT. Measured energy spectra and images obtained are presented.

## 1. Introduction

Portable gamma cameras capable of imaging high energy gamma rays (1–2 MeV) are of interest in a variety of industrial settings. A second generation gamma camera design which improves upon the efficiency of our single aperture camera [1] is presented here. The camera uses a 3 in. square Position Sensitive Photomultiplier Tube (PSPMT) (Hamamatsu, R-2487-05) [2] coupled to a NaI(Tl) scintillator. The incoming gamma ray direction is determined by a segmented collimator [3]. The combination gives rise to a compact and yet efficient gamma camera capable of imaging high energy gamma fields. PSPMTs have recently been extensively used for imaging gamma rays of substantially lower energies [4–9]. In an effort to image higher energy gamma rays, a pinhole collimator with a segmented scintillator attached to the PSPMT was presented in Ref. [10]. In this work we explore using PSPMTs to image high energy gamma rays using a multiple hole collimator.

## 2. Camera design

The assembled camera (without shielding) is shown in Fig. 1. The PSPMT, preamplifier circuit, and scintillator are mounted within a hardened aluminium box. This compact unit is connected to the computer through the trigger and peak detection circuitry board.

### 2.1. Collimator

A segmented collimator with cylindrical holes with diverging axes is employed to determine the directionality of the source distributions. The primary interest in developing this camera is to image radioactivity distributions involving high energy gamma rays over large fields of view. With this application in mind, a segmented collimator was designed with fields of view from adjacent holes that overlap only at infinity (neglecting septal penetration). In a realistic case, due to increasing penetration at higher energies, the distance at which the fields of views overlap decreases with increasing energy of the gamma rays to be imaged.

This collimator has the disadvantage of dead areas (i.e., areas in the source plane which will not be seen in the image plane) when the source distribution is close to the collimator face. However, this dead area rapidly decreases as the source–collimator distance is increased [3].

### 2.2. Scintillator

The scintillator chosen for this camera was a 7.5 cm × 7.5 cm × 1 cm block of NaI(Tl), housed in a machined aluminium can with a 0.2-mm thick entrance window. All the inner faces of the scintillator, except the exit window, are covered with a black, light absorbing coating to prevent light spreading. The interaction efficiency within the scintillator increases as the detector thickness is increased. However, the light spread, due to the isotropic emission of

☆ This work was supported under the U.S. Department of Energy, Robotics for Advanced Reactors, Grant No. DOE-FG02-86NE37969.

* Corresponding author.


*SSDI* 0168-9002(94)00766-7

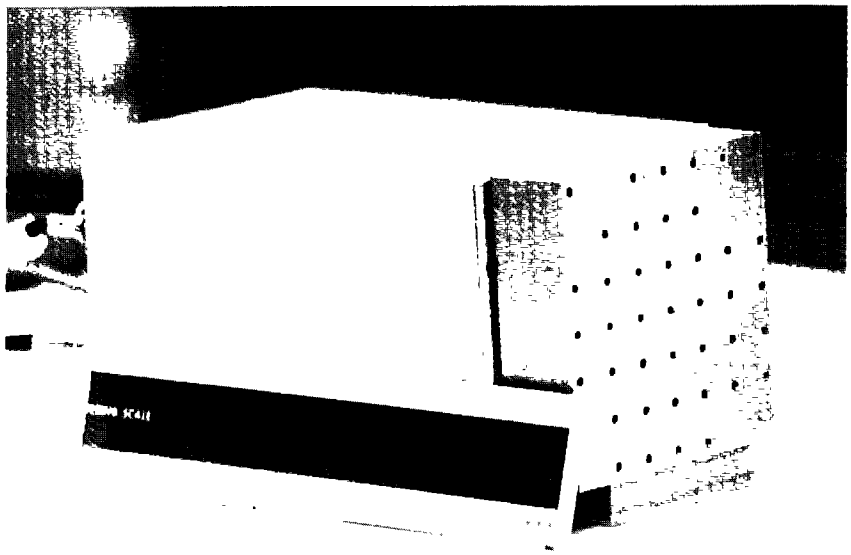

Fig. 1. Photograph of the high energy gamma camera.

photons from the point of gamma ray interaction, also increases with increasing thickness of the scintillator. This spreading leads to broader illumination of the anode crossed wires of the PSPMT. While the centroid of the response remains the same, an increased response will be seen from surrounding locations leading to images of lower contrast. From Monte Carlo studies, a compromise detector thickness of 1 cm was chosen. At this thickness the NaI(Tl) detector has a total interaction efficiency of $\approx 99\%$ for 122 keV and $\approx 25\%$ for 662 keV. The full-energy interaction efficiencies are much lower ($\approx 95\%$ and 6% for 122 keV and 662 keV respectively) than the total interaction efficiencies. At higher energies, efficiencies of the scintillator decrease. The overall efficiency is significantly higher than that displayed by the single shutter first generation camera by virtue of the multiple apertures. A proposed refinement which makes use of pixelated detectors instead of a single slab of detector is described in Ref. [11].

### 2.3. Electronics

A block diagram of the system configuration is given in Fig. 2. A Trigger and Peak detection board was fabricated which enabled the peak values (above a noise threshold) of the four outputs of the PSPMT to be sampled. The sum of these outputs was treated as the trigger pulse for the

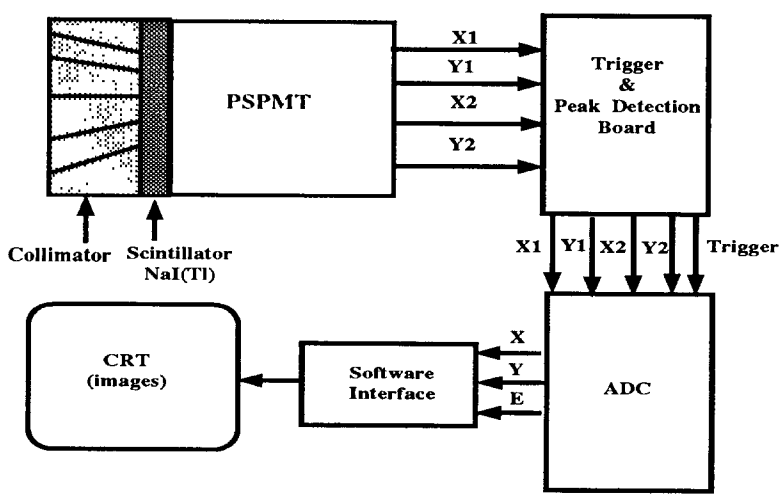


Fig. 2. Block diagram of the high energy gamma camera.

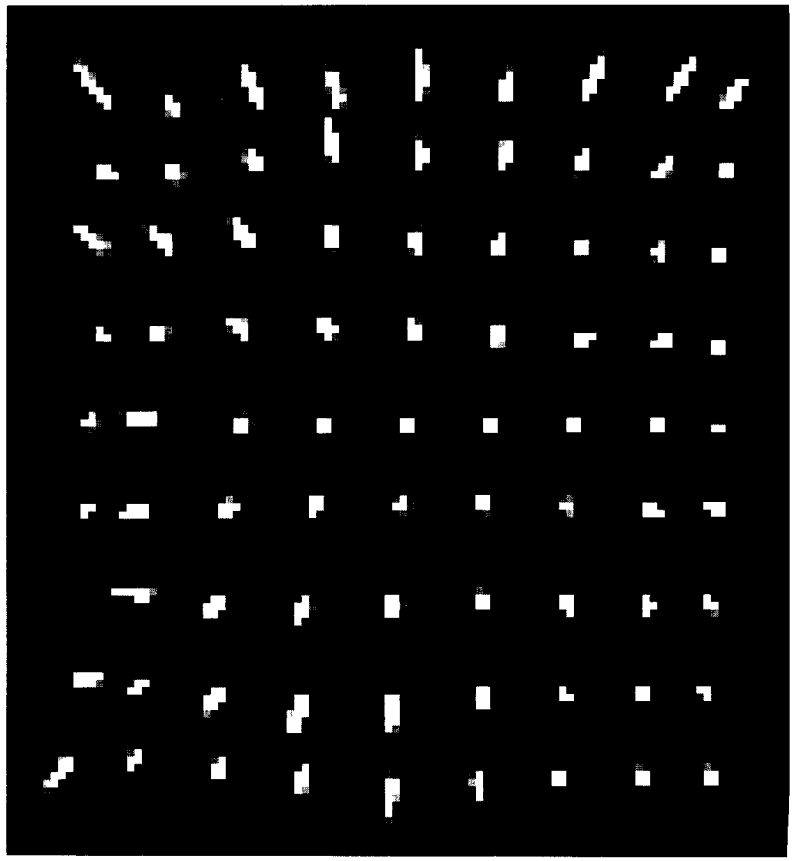

Fig. 3. Image obtained from a fibre optic cable located at various positions along the face of the tube.

Analog to Digital Converter (ADC). The ADC is controlled using an IBM 486-DX PC and the digitized values of the four signals from the PSPMT were stored in the PC. Radiation Monitoring Devices (RMD) has fabricated a commercially available board which also performs the above functions [12]. The raw data files were later transferred to a SUN workstation and were post-processed for the interaction position and the energy deposited by each event.

## 3. PSPMT characterization

The PSPMT was characterized by moving a fibre optic cable, 1 mm in diameter, across the face of the tube. The

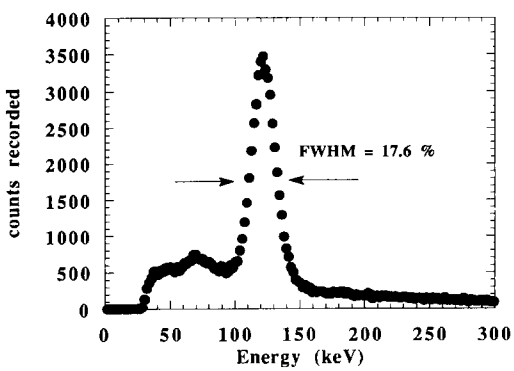


Fig. 4. $^{57}$Co spectrum measured at one position

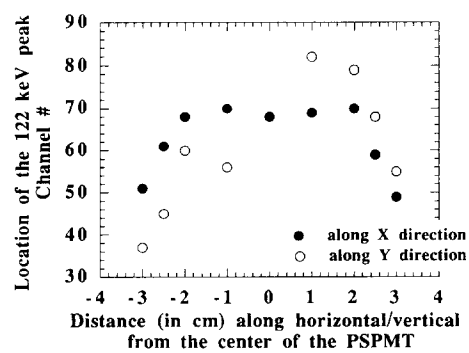


Fig. 5. Variation in sensitivity across the PSPMT.

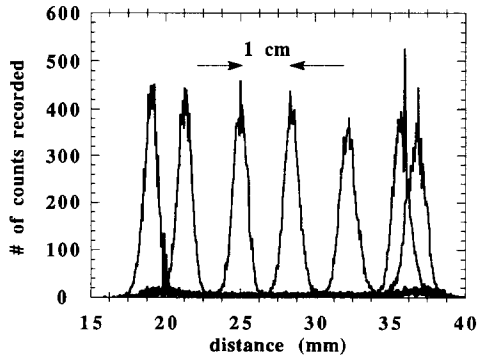


Fig. 6. Spatial resolution of the camera at 122 keV.

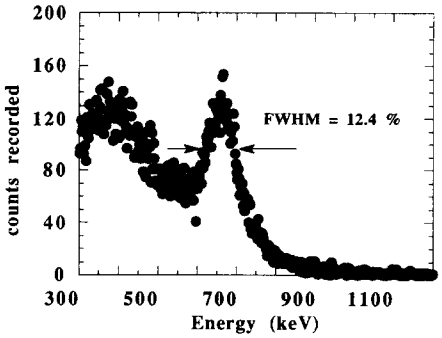


Fig. 8. $^{137}$Cs spectrum measured at one position.

optic cable was illuminated by a green LED. The fibre optic cable was located at various points along a $9 \times 9$ equally spaced grid. The response from the tube is shown in Fig. 3 and shows a characteristic non-uniform response of the tube. Two factors to be accounted for when imaging with a PSPMT are the non-linear PSPMT response and edge compression effect. The tube displayed good linearity over most of the area of the photocathode (60 mm $\times$ 55 mm) and showed non-linearity at peripheral regions. Knowing the response of the tube to LED sources located at various known positions an offset correction

$$r_{\text{corrected}} = \frac{(r_{\text{measured}} - r_{\text{offset}})}{r_{\text{gain}}},$$

where $r_{\text{offset}}$ and $r_{\text{gain}}$ are obtained from the LED calibration, was performed to calibrate interaction position of the tube response. The edge compression effect refers to the peripheral area where two interaction positions yield the same tube output. A method suggested for treating this problem can be found in Ref. [6].

## 4. Camera performance

### 4.1. Low energy

Using a 1 mm collimated $^{57}$Co (122 keV) source, the energy spectrum recorded by the gamma camera at the

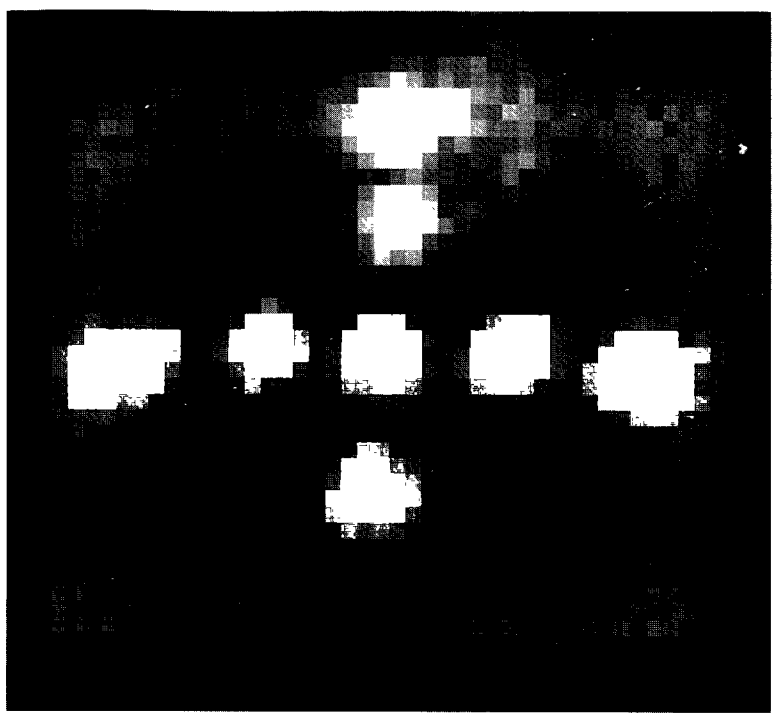

Fig. 7. Uncorrected image of a grid of $^{57}$Co point sources, located 1.0 cm apart.

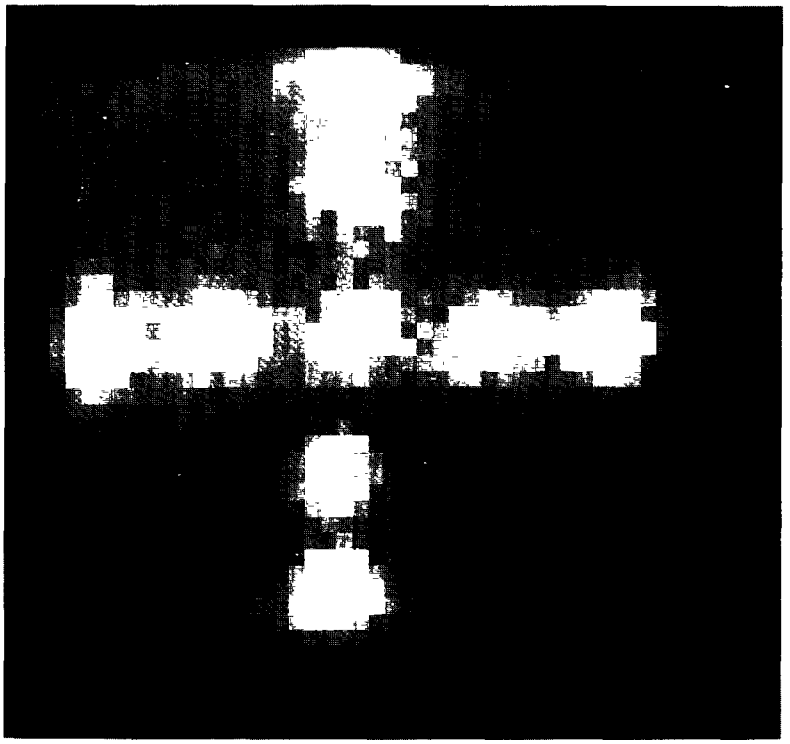

Fig. 9. Uncorrected image of a grid of $^{137}$Cs point sources, located 1.07 cm apart.

center of the tube is shown in Fig. 4. The full energy peak shows a resolution between 17% and 23% FWHM. The gain of the PSPMT varies across its entire face. By moving the same collimated source, the gain variation of the tube along the $X$ and $Y$ directions was found to vary as shown in Fig. 5. The variation in the gain is non-intuitive along both $X$ and $Y$ directions. The spatial response in the $X$ direction was between 2.8 mm and 3.2 mm as shown in Fig. 6. Using the known sensitivity, a window was set around the full energy peak of $^{57}$Co and yielded the image shown in Fig. 7. This image was obtained using a collimator with a hole diameter of 0.1 cm and a hole separation of 1.0 cm.

### 4.2. Medium energy

For a $^{137}$Cs (662 keV) source, the measured energy spectrum at the center is shown in Fig. 8 with an energy resolution of 12% FWHM. An image obtained using point $^{137}$Cs sources is shown in Fig. 9. This image was obtained using a collimator with a hole diameter of 0.36 cm and a hole separation of 1.07 cm. Comparing to Fig. 7, note that a greater number of pixels close to the source location now

Table 1
Measured performance parameters of the camera

| | This camera 7.5 cm × 7.5 cm × 1 cm NaI(Tl) | | | Bare detector 7.6 cm × 7.6 cm NaI(Tl) | |
|---|---|---|---|---|---|
| | Spatial resolution (mm) | Energy resolution (% FWHM) | Intrinsic efficiency (%) | Energy resolution (% FWHM) | Intrinsic efficiency (%) |
| 122 keV | 2.9 | 17.6 | 99 | 15 | 99 |
| 662 keV | 5.4 | 12.4 | 25 | 7 | 84 |

display a higher intensity. This is due to the larger diameter of the holes and higher energy of the gamma rays imaged.

## 5. Conclusions

A gamma camera was fabricated using NaI(Tl) crystal and PSPMT and tested at 122 keV and 662 keV. The camera parameters measured at the center are summarized in Table 1. We are currently investigating ways to improve these values, handle the dead areas, and account for the edge compression effects for unknown multiple energy and spatially extended sources.

## References

[1] T.A. DeVol, D.K. Wehe and G.F. Knoll, Nucl. Instr. and Meth. A 299 (1990) 495.
[2] H. Kume and S. Muramatsu, IEEE Trans. Nucl. Sci. NS-33 (1986) 359.
[3] S.V. Guru, J.D. Valentine, D.K. Wehe and G.F. Knoll, Monte Carlo modelling of a multiple-hole collimator for high energy gamma-ray imaging, accepted for publication in IEEE Trans. Nucl. Sci.
[4] R.H. Redus, V. Nagarkar, L.J. Cirignano, W. McGann and M.R. Squillante, IEEE Trans. Nucl. Sci. NS-33 (1992) 1354.
[5] Z. He, A.J. Bird, D. Ramsden and Y. Meng, IEEE Trans. Nucl. Sci. NS-40 (1993) 447.
[6] N.J. Yasillo et al., A single tube miniature gamma camera, presented at IEEE Nuclear Science Symp., 1993.
[7] T.D. Milster et al., J. Nucl. Medicine 31 (1990) 632.
[8] N.J. Yasillo, R.N. Beck and M. Cooper, IEEE Trans. Nucl. Sci. NS-37 (1990) 609.
[9] C.E. Ordonez et al., Simulation of imaging with NaI(Tl) crystals and position sensitive photomultiplier tubes, presented at IEEE Nuclear Science Symp., 1993.
[10] R.H. Redus, M.R. Squillante, J. Gordon, D.K. Wehe and G.F. Knoll, these Proceeding (1994 Symposium on Radiation Measurements and Applications, Ann Arbor, MI, USA) Nucl. Instr. and Meth. A 353 (1994) 324.
[11] Z. He, A. Truman, S.V. Guru, D.K. Wehe, G.F. Knoll and D. Ramsden, Portable wide-angle γ-ray vision systems, submitted to IEEE Trans. Nucl. Sci.
[12] Radiation Monitoring Devices, Position Sensitive Photomultiplier Interface System, private communication, 1993.